Supplementary Data

Supplementary Materials and Methods

Cell culture

Umbilical cord-lining-derived mesenchymal stem cells (CL-MSC) isolated from the subamnion of the umbilical cord were provided by CellResearch Corporation Pte Ltd., Singapore [1]. CL-MSC were maintained in proprietary serum-free media containing DMEM-F12-CMRL1066 (GIBCO®; Life Technologies Corporation) with supplement of albumin, insulin, bFGF, TGFβ1 (all from R&D Systems, Inc.) and LIF, and incubated at 37°C in 5% humidified CO_2. CL-MSC were subcultured upon reaching confluency of 80%–85% by mechanically lifting the cells from the surface of tissue culture flask using a cell lifter (Costar®; Corning Life Sciences).

Human umbilical vein endothelial cells (HUVEC) were cultured in endothelial cell medium (ScienCell Research Laboratories). Human dermal fibroblast adult (HDFa) were maintained in medium 106 with low serum (GIBCO).

Multipotent capacity of CL-MSC

For CL-MSC adipogenic, chondrogenic, and osteogenic differentiation, 6×10^5 cells in growth medium PTT-4 were plated in 6-well plates (Techno Plastic Products AG) and incubated at 37°C in 5% humidified CO_2. After 24 h in culture, the appropriate differentiation medium was added (Lonza). Differentiation medium was changed twice a week for 3 weeks. Next, cells were stained for adipogenic (Oil Red O and hematoxylin counterstaining), chondrogenic (Alcian Blue), and osteogenic (Von Kossa) differentiation as described elsewhere [1–3]. Images were acquired using an Olympus IX71 microscope (Olympus).

Production of lentiviral vectors and generation of fluorescent-bioluminescent CL-MSC

Lentiviral vectors pWPT-GFP and pLVX-LUC-puro, pseudotyped with the VSV-G, and packaged with plasmid pPax2 were generated by calcium phosphate-mediated transfection of 293T cells. Cells were plated in 10-cm plate at a density of 8×10^6 cells in 10 mL of Dulbecco's modified Eagle's medium (DMEM, high-glucose; GIBCO) supplemented with 10% FBS, 1% penicillin/streptomycin. Lentivirus vector, packaging, and envelope glycoprotein plasmids were mixed together with 1 mL of 0.25 M CaCl2 and 1×BES (*N*,*N*-Bis(2-hydroxyethyl)-2-aminoethanesulfonic acid), incubated for 30 min and added to 293T cells. Transfection medium was replaced by complete medium 8 h later. Twenty-four hours after the medium change, the vector-containing medium was collected and filtered through a 0.45-μM pore size filter and used fresh or stored at −80°C. For transduction, 10^5 CL-MSC cells (at either passage 3 or 4) were seeded into each well of 6-well plates. Transductions were performed in either pLVX-LUC-puro, pWPT-GFP alone, or in combination using equal volumes of viral supernatant (0.25 and 0.5 mL of each) in the presence of 8 μg/mL Polybrene (Sigma). The medium was changed to complete culture medium 12–16 h after addition of lentivirus. Cells transduced with pLVX-Luc-puro and pLVX-Luc-puro with WPT-GFP (*CL-MSC-GFP-Fluc)* were selected with 0.8 μg/mL of puromycin.

CL-MSC immunophenotype analysis by flow cytometry

CL-MSC-*GFP-Fluc* (1×10^6 cells) were harvested at passage 5–6 from culture dishes by trypsinization and washed with phosphate-buffered saline (PBS) containing 1% bovine serum albumin (BSA; Invitrogen). Cells were incubated with suitable combinations of the following anti human monoclonal antibodies or isotype-matched control monoclonal antibodies (all from BD Pharmigen™) unless stated otherwise: CD14-APC-Cy7 (mouse IgG2b, k clone MphiP9), CD15 (mouse IgM, k clone HI98), CD29-APC (mouse IgG1, k clone MAR4), CD31-Alexa Fluor® 647 (mouse IgG2a, k clone M89D3), CD34 (mouse IgG1 clone 58; AbD Serotec), CD44 (mouse IgG1, k clone L178), CD45-APC (mouse IgG1 clone HI30; Molecular Probes®, Life Technologies Corporation), CD73 (mouse IgG1, k clone AD2), CD 90 (mouse IgG1, k clone 5E10), CD105 (mouse IgG1, k), CD117 (mouse IgG1 clone 104D2), mouse IgG1, k-APC isotype control (mouse, MOPC-21), IgM, κ isotype control (mouse, clone G155–228), IgG2a, k-Alexa Fluor 647 isotype control (mouse, clone G155–178), IgG2b, k-APC-Cy7 isotype control (mouse, clone 27–35).

Cells were then fixed with 1% paraformaldehyde (PFA) and analyzed on a BD FACSCanto™ flow cytometer (BD Biosciences). Data were analyzed with FlowJo software version 10.0.4 (Tree Star, Inc.).

Western blot analysis of VEGF in CL-MSC angiogenic spheroids

To assess VEGF levels in angiogenic spheroids, uncoated CL-MSC spheroids were harvested after 3 days of culture in hanging drops, whereas coated spheroids were harvested either 2 days after co-culture of CL-MSC spheroids with HUVEC in hanging drops (coated spheroids day 5) or after 4 days in co-culture (coated spheroids day 7), and washed with PBS. Lysis buffer (50 mM Tris-HCl at pH 7.5, 150 mM NaCl, 5 mM EDTA, 1% Nonidet P-40 (NP-40) buffer and 10% glycerol) containing a protease inhibitor (Roche Diagnostics) was used to solubilize cells from monolayer cultures as follows: CL-MSC-*GFP-Fluc*, HUVEC and HDFa (used as negative control), or from spheroids as described above. Fifty microgram of proteins were separated by SDS-PAGE and subsequently transferred onto PVDF membranes (Immobilon-P; Millipore Corporation). Membranes were incubated with rabbit anti VEGF antibody (1:500; Merck Millipore) for 2 h at room temperature, followed by incubation with rabbit anti GAPDH antibody (1:2,500; Abcam) for 1 h at room temperature. Membranes were then exposed using GelDoc (Bio-Rad Laboratories, Inc.). Experiments were done in triplicate.

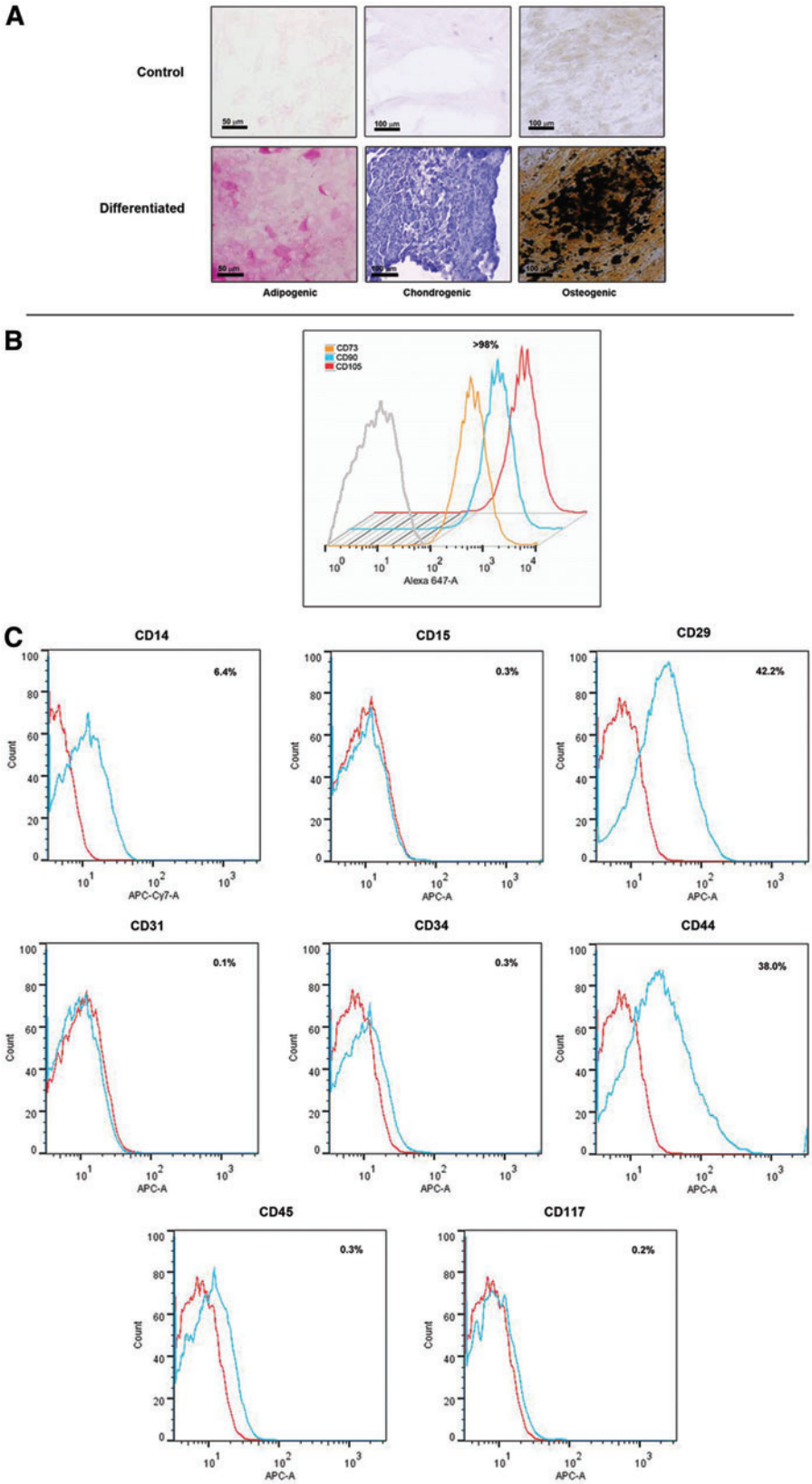

SUPPLEMENTARY FIG. S1. Characterization of human CL-MSC. **(A)** Oil Red O staining Alcian blue, and Von Kossa, (100×) and demonstrating CL-MSC-GFP-fluc multi-lineage differentiation potential. **(B, C)** Surface antigen expression of CL-MSC-GFP-fluc as analyzed by flow cytometry. All markers were expressed in a cellular percentage. **(B)** *Gray* histogram represents the isotype control for CD73, CD90, and CD105. **(C)** *Blue* histograms represent the antigen whereas *red* histograms correspond to the isotype control. GFP, green fluorescent protein; fluc, firefly luciferase. CL-MSC, cord-lining mesenchymal stem cells.

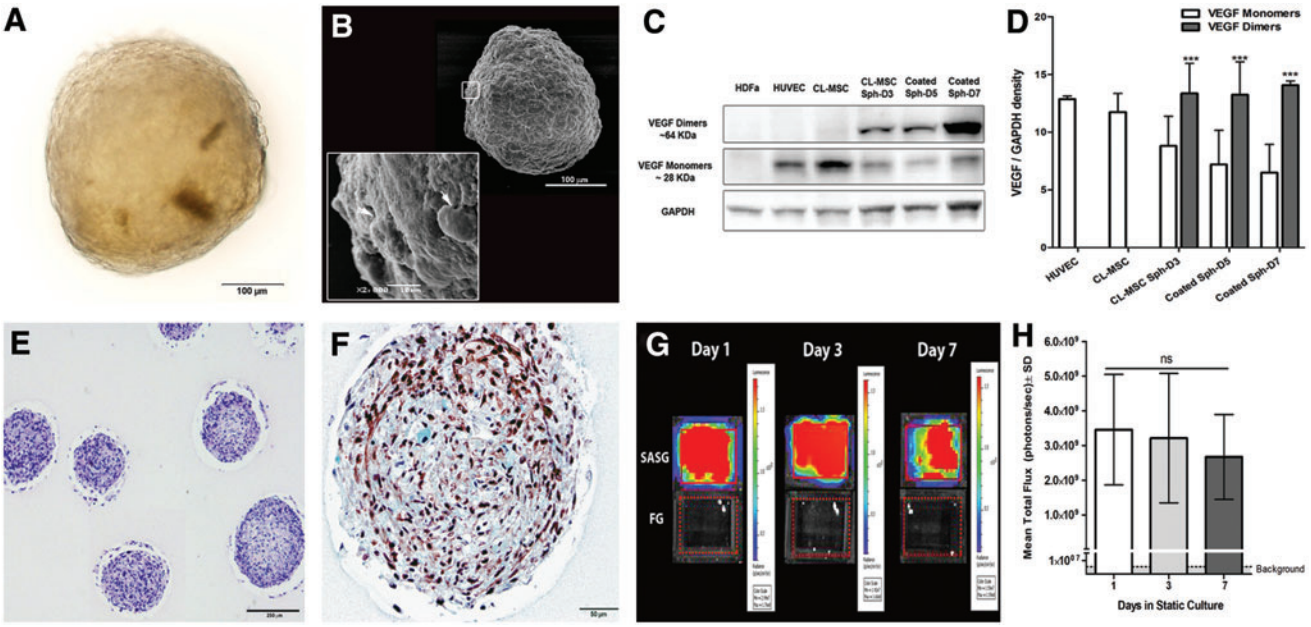

SUPPLEMENTARY FIG. S2. **(A)** Spheroids after 7 days of gravity-enforced culture. Compact and well delimited spheroids (250–300 μm diameter) were formed, in which cells were not discriminable by light microscopy. **(B)** Scanning electron microscopy of CL-MSC-GFP-fluc and HUVEC angiogenic spheroids after 7 days in hanging drops. Low-magnification image (250×) shows compact spheroids with extensive extracellular matrix that only allows a few individual cells distinguishable on the surface. High-magnification image of *inset* (2,000×) shows cell–cell tight junctions (*arrows*). **(C, D)** Western blot analysis of VEGF protein level in monolayer cultures (HDFa, HUVEC, and CL-MSC) and in uncoated CL-MSC spheroids after 3 days in hanging drop culture (CL-MSC Sph-D3), or coated spheroids after 5 (Coated Sph-D5) and 7 days in culture (Coated Sph-D7). Expression of VEGF monomers was comparable between HUVEC and CL-MSC-*GFP-fluc* cultured in monolayers. After assembly of CL-MSC-*GFP-fluc* in three-dimensional spheroids, VEGF monomers were reduced and VEGF dimers increased compared to both CL-MSC and HUVEC monolayer cultures (***$P < 0.001$). **(E)** H&E staining showing distribution of angiogenic spheroids within fibrin grafts (SASG). **(F)** Masson's trichrome staining of SASG revealed production of extracellular matrix (*blue*) within the spheroids. **(G, H)** BLI of SASG at 1, 3, and 7 days under static culture showed nonsignificant changes in donor CL-MSC-*GFP-fluc* viability. VEGF, vascular endothelial growth factor; HDFa, human dermal fibroblasts adult; HUVEC, human umbilical vein endothelial cells; SASG, subamnion-CL-MSC angiogenic spheroid-enriched grafts; SD, standard deviation; H&E, hematoxylin and eosin; BLI, bioluminescence imaging.

In vitro evaluation of cell viability within subamnion-CL-MSC angiogenic spheroids-enriched grafts

Because spheroids may have less access to oxygen and nutrients within subamnion-CL-MSC angiogenic spheroids-enriched grafts (SASG) maintained under static culture conditions, viability of donor cells within SASG was assessed in vitro via bioluminescence imaging (BLI) after 1, 3, and 7 days in culture. Each condition was evaluated in three different experiments ($n = 3$/time point). In vitro BLI was done using a Xenogen IVIS Lumina System (Caliper Life Sciences) as previously described by us [4]. Bioluminescence was quantified in units of photons per second total flux (p/s). Data were analyzed using Living Imaging Software version 3.2 (Caliper Life Sciences).

Detection of apoptotic cells within SASG

After 1, 3, and 7 in culture, and after in vitro BLI SASG were fixed in 10% buffered formalin for 2 h, embedded in optimal cutting temperature (OCT) compound (Tissue-Tek®; Sakura Finetek) and frozen at −80°C. To detect apoptotic cells within SASG, 10 μm cryosections were stained using an active Caspase-3 antibody (Rabbit polyclonal; Abcam) as previously described [4]. *z*-Stack images were obtained using a Nikon A1R confocal microscope (Nikon) and subsequently processed using NIS-Elements software (v 3.1). Sections from three different experiments were analyzed. Cells were counted using Image J software (1.42q; National Institutes of Health) and the percentage of active caspase 3-positive cells was calculated.

Scanning electron microscopy of subamnion-MSC angiogenic spheroids

For scanning electron microscopy, angiogenic spheroids were fixed with 2.5% glutaraldehyde in 0.1 M cacodylate buffer (pH 7.2). Subsequently, samples were incubated in 1% osmium tetraoxide in the same buffer. Spheroids were washed and dehydrated by graded ethanol series, followed by critical-point drying with CO_2. Next, spheroids were mounted on aluminum stubs, and coated with a 20-nm-thick layer of gold. The samples were examined under a scanning electron microscope JEOL JSM-5600LV (Jeol Ltd.).

In vivo and ex vivo BLI

To investigate in vivo CL-MSC donor cell viability following SASG implantation, we performed BLI using a Xenogen-IVIS® Lumina imaging system (Caliper Life Sciences) as previously described [5]. All rats from the SASG and SASG-

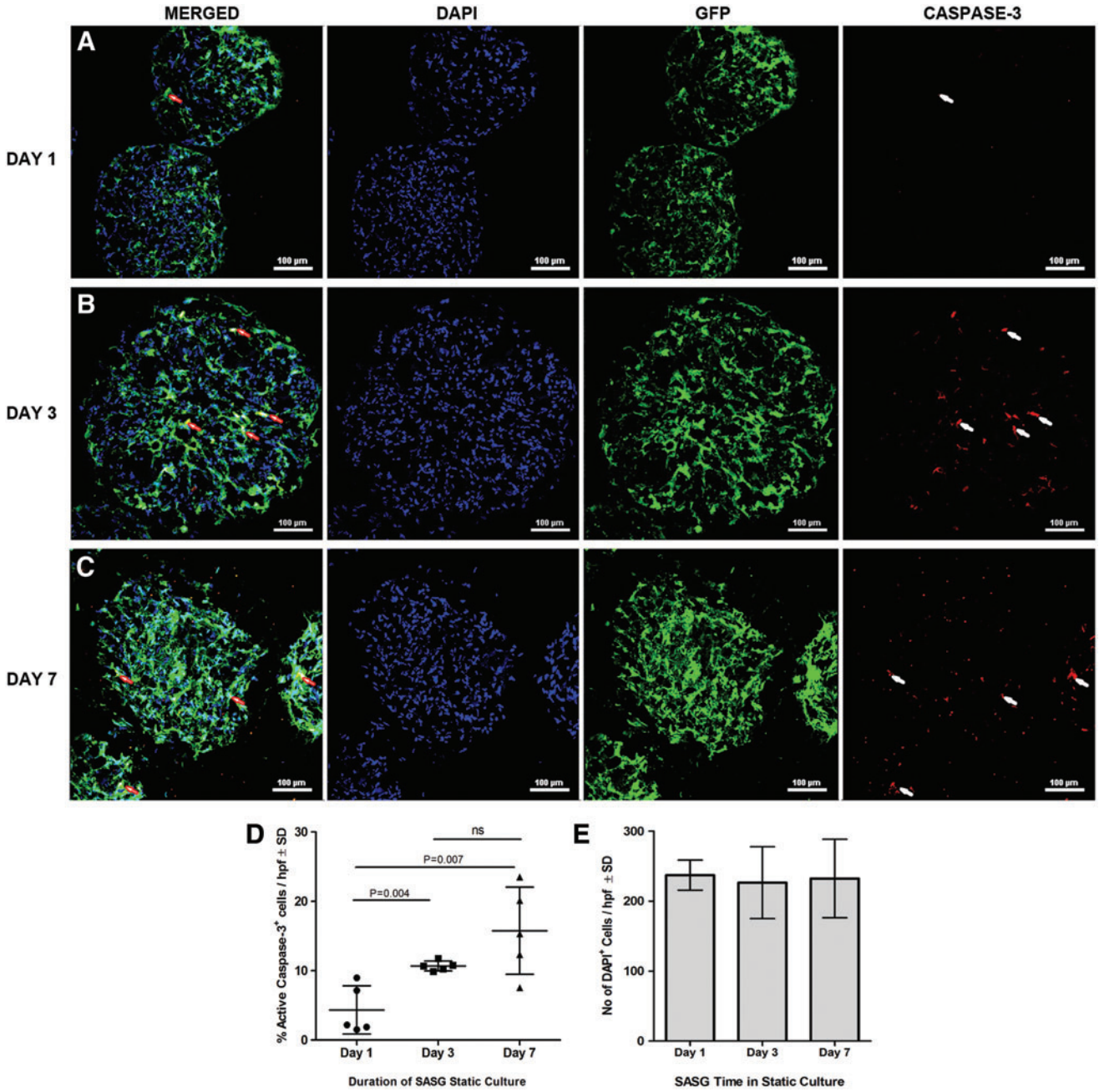

SUPPLEMENTARY FIG. S3. Apoptosis assessment within SASG in vitro. Representative confocal micrographs of active caspase-3 staining (red) in CL-MSC-*GFP-fluc*/HUVEC spheroids embedded in FGs after 1 **(A)**, 3 **(B)**, and 7 **(C)** days in culture; (100×). *Arrows* are pointing at some caspase 3-positive cells. CL-MSC-*GFP*$^+$ (*green*), DAPI$^+$ nuclei (*blue*); scale bars indicate 100 µm. **(D)** The percentage of apoptotic cells within the spheroids was significant at 3 and 7 days in culture, relative to day 1. **(E)** Determination of cell number (DAPI$^+$ cells) within spheroids revealed that cell number within spheroids during SASG static culture from day 1 to 7 remained stable. FG, fibrin graft.

video-assisted thoracoscopic surgery (VATS) groups were imaged on days 1, 3, 7, and 14, following treatment. To locate surviving CL-MSC-*GFP-fluc* 4 weeks after treatment, hearts were imaged ex vivo immediately after animal euthanasia. Following a gentle rinse with ice-cold DPBS, explanted hearts were placed in 6-well plates, submerged in 150 mg/mL working solution of D-luciferin (Caliper Life Sciences) in DPBS and imaged for 5 min at 30-s intervals. Data were analyzed using Living Imaging Software version 3.2.

Subamnion-CL-MSC angiogenic spheroids histology

After in vitro studies, SASG were washed in PBS, fixed in 10% buffered formalin and embedded in paraffin or in OCT compound (Tissue-Tek; Sakura Finetek). To identify the spheroids embedded within the graft, 10-µm sections were stained with hematoxylin and eosin (H&E) and Masson's thrichrome.

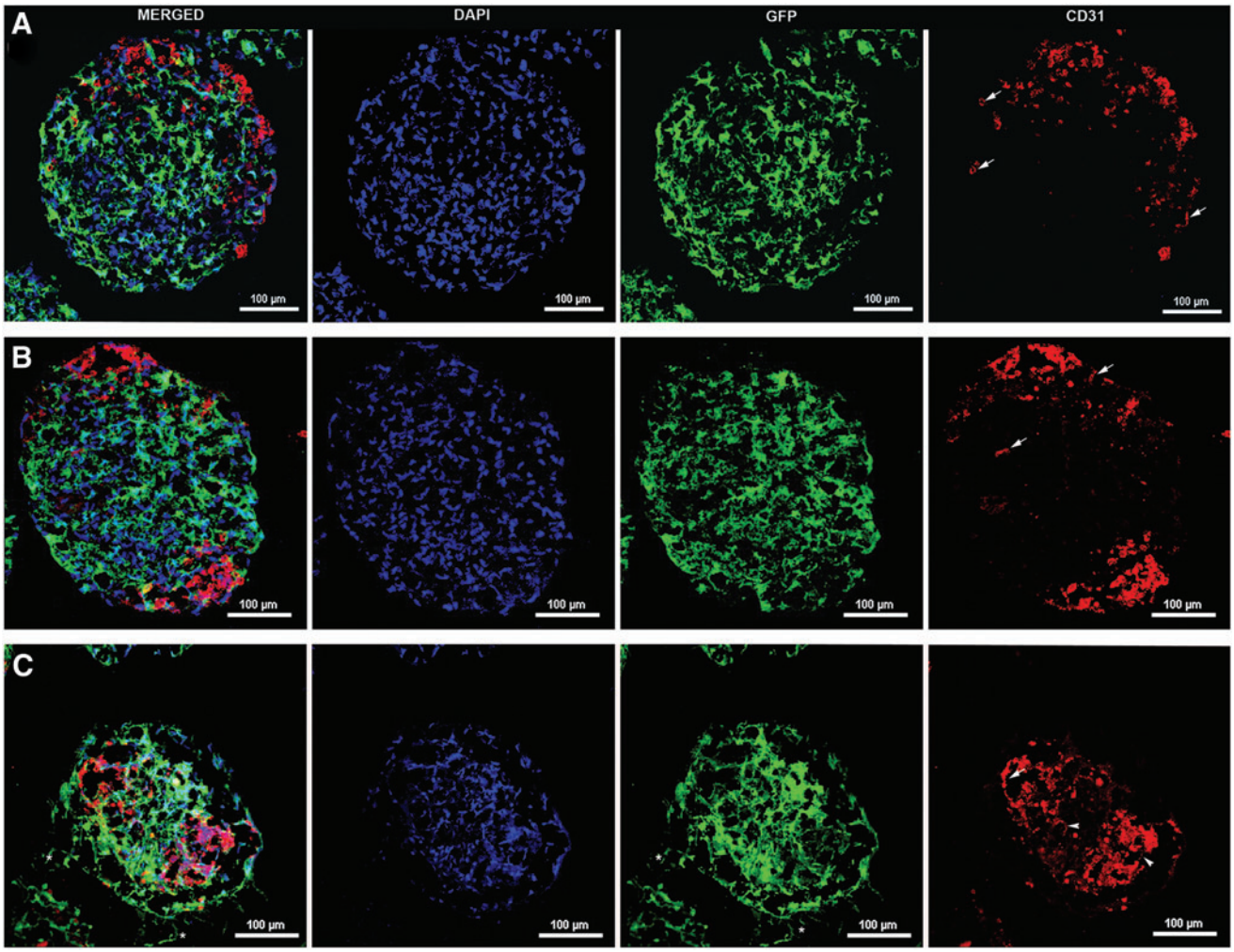

SUPPLEMENTARY FIG. S4. Confocal micrographs of SASG (100×) at 1 **(A)**, 3 **(B)** and 7 days **(C)** in vitro, stained for human CD31. **(A–C)** Donor CL-MSC-*GFP-fluc* (*green*) adopted a MSC in vivo-like elongated shape inside the spheroids and organized into compact cellular networks. HUVEC (*red*) were found in close contact with CL-MSC at all time-points in static culture and assembled into branches capillary-like structures (*arrows*) while penetrating the spheroid's core [13]. **(C)** By day 7 of SASG static culture, HUVEC displayed sprouting (*arrowheads*), whereas some CL-MSC started to migrate outside of the spheroid into the fibrin matrix (*asterisk*). Scale bar, 100 µm.

Immunofluorescence of SASG

Distribution of HUVEC within the spheroids after SASG were maintained in static culture for 1, 3, or 7 days was evaluated through immunohistochemical staining using an antibody against human CD31 (mouse monoclonal; Dako). Alexa Fluor-594 (Molecular Probes, Life Technologies Corporation) was used as secondary antibody. A GFP-Alexa Fluor-488 antibody (Molecular Probes) was used to identify CL-MSC-*GFP-fluc* within SASG. Nuclei were counterstained with 4′,6-diamidino-2-phenylindole (DAPI) (Molecular Probes).

Echocardiography

Transthoracic echocardiography was performed by a blinded investigator (LHL) at baseline, and 2 and 6 weeks following myocardial infarction (i.e., 4 weeks after treatment), using a Vivid 7 Dimension ultrasound system equipped with a broadband 10S transducer (GE VingMed) [5]. LV internal diameter and wall thickness during diastole and systole were measured. End-diastolic and end-systolic cross-sectional areas were measured from the parasternal short-axis view and fractional area change (FAC) calculated as FAC % = [(end-diastolic area − end-systolic area)/end-diastolic area] × 100, with end diastole defined as the peak of the R wave, and end systole defined as the end of the T wave. LV volumes were calculated using a modified Teichholz formula as described elsewhere [6]. Ejection fraction (EF %) was calculated as [(LV end-diastolic volume − LV end-systolic volume)/LV end-diastolic volume] × 100. Offline measurements of LV dimensions and areas were made from three consecutive cardiac cycles using EchoPac software (version 6; GE VingMed).

Hemodynamic measurements

Left ventricular (LV) pressure and volume measurements were performed 4 weeks post-treatment as described previously [5]. Briefly, after anesthesia, intubation, and mid-thoracotomy, the ascending aorta was exposed and a 2-mm transient-time flow probe was positioned around of it for cardiac output measurement (Transonic Systems, Inc.). Next, the LV was cannulated through the apex with a pressure

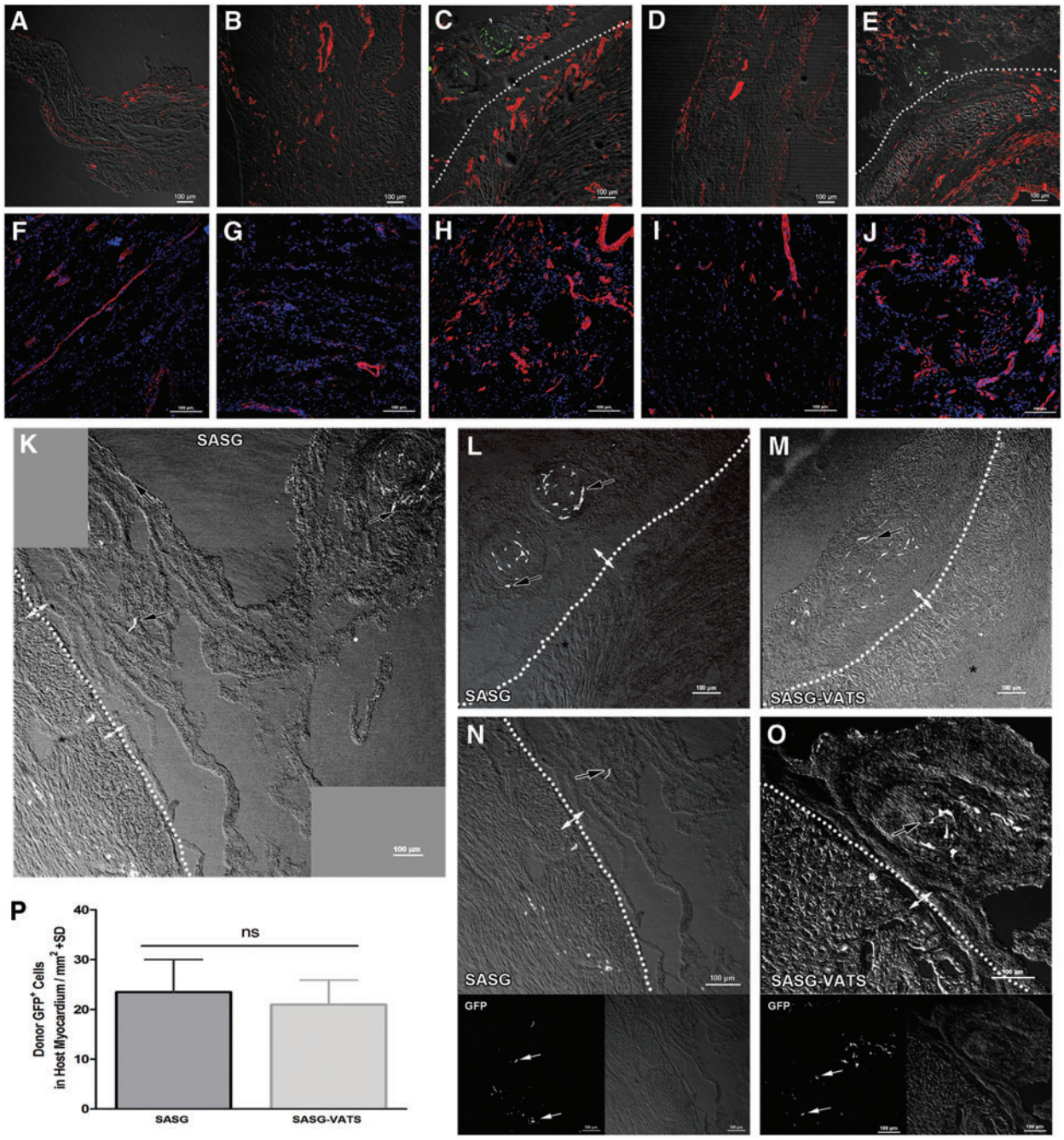

SUPPLEMENTARY FIG. S5. α-SMA expression in the native myocardium. Representative confocal micrographs of **(A, F)** untreated rat hearts (MI), and those treated with **(B, G)** FG through thoracotomy, **(C, H)** subamnion angiogenic spheroid-enriched grafts implanted through lateral thoracotomy (SASG), **(D, I)** FG implanted by minimally invasive VATS (FG-VATS), and **(E, J)** SASG delivered through VATS (SASG-VATS), after 6 weeks of myocardial injury. α-SMA$^+$ blood vessels are labeled in *red*, donor GFP$^+$ cells in *green* and DAPI$^+$ nuclei in *blue*. *Upper panel* **(A–E)** corresponds to *xy* confocal micrographs merged with the transmitted light channel to identify underlying LV scar and graft areas (40×); *white arrowheads* pointing out at spheroids embedded within FG. *Lower panels* **(F–J)** correspond to micrographs taken in the LV scar area (200×). Abundant α-SMA$^+$ blood vessels were found within the scar area of SASG and SASG-VATS groups compared to MI and their respective FG/FG-VATS controls. Also, arterioles were seen infiltrating the fibrin grafts and surrounding spheroids. Scale bar indicates 100 μm. Donor CL-MSC-GFP$^+$ cells within the epicardial graft and LV scar area of SASG **(K, L, N)** and SASG-VATS **(M, O)**. CL-MSC-GFP$^+$ (*white*) were found either within the spheroids extracellular matrix or fibrin graft (*black arrows*). GFP$^+$ cells within the graft area were observed in all treated animals. Yet, CL-MSC-GFP$^+$ within the host myocardium (adjacent to the graft area) were found in around 62% of SASG and 50% of SASG-VATS heart sections **(N, O)**. Quantification of the number of donor GFP$^+$cells/mm^2 of LV scar area contiguous to the graft ($n = 4–5$/group) showed no difference between SASG and SASG-VATS **(P)**. Joint of the epicardium and the epicardial graft is indicated by double *white arrows*, while *asterisks* indicate the LV scar. *Dotted line* indicates host/graft interface. Confocal *xy* micrographs merged with the transmitted light channel. Scale bars, 100 μm. VATS, video-assisted thoracoscopic surgery; α-SMA$^+$, alpha-smooth muscle actin positive; LV, left ventricular.

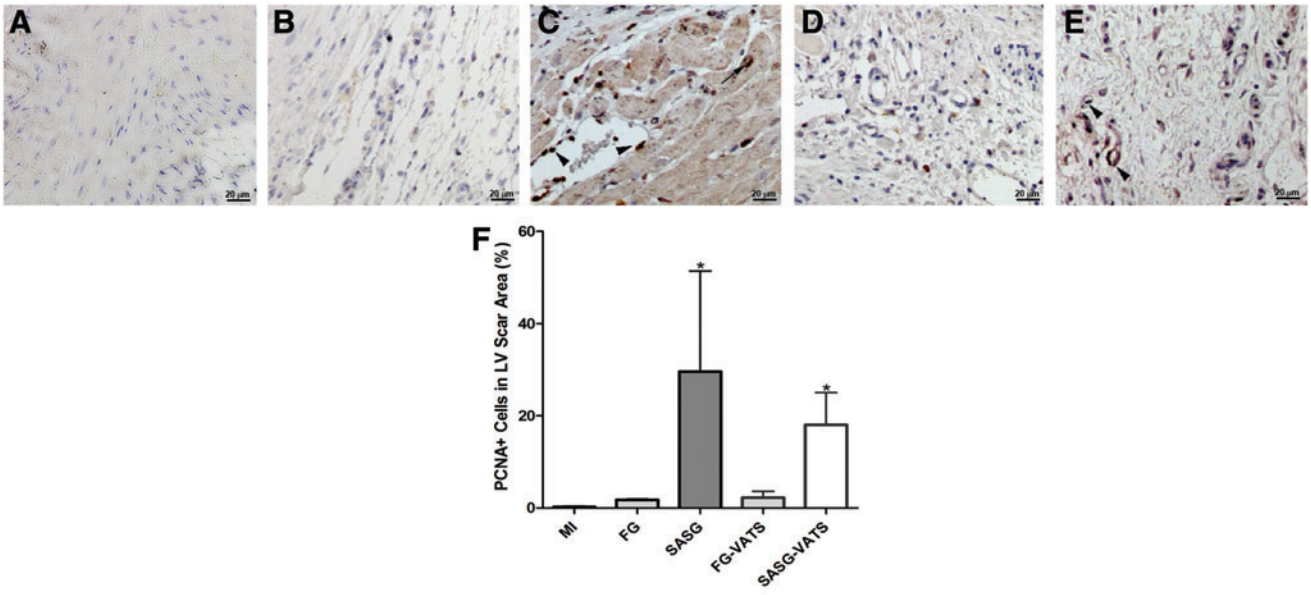

SUPPLEMENTARY FIG. S6. PCNA staining in the LV scar area of **(A)** untreated rat hearts (MI), and those treated with **(B)** FG through thoracotomy (FG), **(C)** subamnion angiogenic spheroid-enriched grafts implanted through lateral thoracotomy (SASG), **(D)** FG implanted by VATS (FG-VATS), and **(E)** SASG delivered through VATS (SASG-VATS), 6 weeks after myocardial injury (200×). **(F)** SASG and SASG-VATS-treated hearts had elevated percentage of $PCNA^+$ proliferating cells in the LV scar area compared to MI (*$P<0.05$, respectively). According to their morphologic appearance, $PCNA^+$ cells were located predominantly in blood vessels (*arrowheads*) of both SASG and SASG-VATS and only in scarce cardiomyocytes of SASG-treated hearts **(***black arrow* in **C)**. PCNA, proliferating cell nuclear antigen.

transducer catheter (Millar Micro-Tip® model SPC-721; Millar, Inc.). Pressure and aortic flow waves were recorded with the Powerlab 8/30 data acquisition system (ADInstruments Pty Ltd.). Data were analyzed using Lab Chart Pro software (version 7.0; ADInstruments).

Left ventricular infarct size and vascularization

Infarct size was determined using Masson's Thrichrome-stained heart cross-sections from all animals which were imaged using a Nikon Eclipse Ti microscope (4×objective), and a motorized stage operated with Nikon NIS-Elements AR 3.2 software. Collected images of the whole section were automatically stitched together by the NIS-Elements software. The percentage of scarred LV wall was determined using midline length measurement (calculated by dividing the midline length of the infarcted LV wall by the midline length of total LV wall) [7] using a semi-automated software (MIQuant) [8]. LV regions with collagen deposition >50% of the thickness of the LV wall were considered for infarct midline calculation [7]. Epicardial tissue corresponding to the implanted graft was excluded from these measurements.

To identify proliferating cells within the LV scar area, proliferating cell nuclear antigen (PCNA) staining was done on paraffin-stained sections according to the manufacturer's instructions (PCNA staining kit; Invitrogen™, Life Technologies Corporation), and counterstained with hematoxylin. PCNA positive and negative cells were counted using Image J software (1.42q; National Institutes of Health), followed by calculation of the percentage of $PCNA^+$ cells in images taken from six random microscopic fields (100×).

After hemodynamic measurements, three animals from each group underwent direct labeling of the blood vessels by cardiac perfusion with a lipophilic carcocyanide dye, which incorporates into endothelial cell membranes upon contact with 1,1′-dioctadecyl-3,3,3′,3′-tetramethylindocarbocyanine perchlorate (DiI) [5,9]. LV vascularization was evaluated in 20-μm cryosections through 0.5 μm *z*-stack imaging and detection of DiI+blood vessels with a Nikon A1R confocal microscope (Nikon). Immunohistochemical staining of blood vessels within the LV scar area was performed in 2 consecutive 5-μm cryosections (cross-sections, $n=4$–5 animals/group) using a ubiquitous marker for rat endothelial cells [Rat endothelial cell antigen (mouse anti-RECA-1), 1:50 monoclonal; HyCult biotechnologt b.v]. Individual $RECA^+$ blood vessel counts were then made on a 200×field (20× objective and 10×ocular; equivalent to 0.7386 mm^2/200× field). Arterioles within the LV scar area and the implanted grafts were also visualized through immunohistochemical staining in 2 consecutive 5-μm heart cryosections using an antibody against smooth muscle actin (monoclonal, clone 1A4; Sigma). An antibody against α-sarcomeric actin was used to identify cardiac differentiation of donor CL-MSC [mouse monoclonal, Clone alpha-Sr-1 (Dako), whereas an antibody against human endoglin (CD105, SC-19790; Santa Cruz Biotechnology, Inc.)] was used to identify donor HUVEC within grafts. Alexa Fluor-594 and Alexa Fluor-350 (Molecular Probes) were used as secondary antibodies and nuclei were stained with DAPI (Molecular Probes). CL-MSC within implanted grafts or the ischemic myocardium was identified using a GFP-Alexa Fluor-488 antibody. Quantification of the amount of donor CL-MSC-GFP^+ (number of cells/mm^2) detected within the LV scar area was done in confocal micrographs from five fields (100×) taken at the graft/host myocardium interface ($n=5$ in SASG group and $n=4$ in SASG-VATS group). *z*-Stack images from all sections

Supplementary Table S1. Comparison of LV Remodeling and Function Between Infarcted Untreated Rats (MI), FG-, Human SASG-, FG-VATS-, and SASG-VATS-Treated Rats, by Two-Dimensional Echocardiography, Before (Baseline), and 2 and 6 Weeks After Myocardial Injury

	MI (n = *8*)	*FG* (n = *8*)	*SASG* (n = *8*)	*FG-VATS* (n = *7*)	*SASG-VATS* (n = *8*)
IVSd (cm)					
Baseline	0.15 ± 0.02	0.15 ± 0.01	0.15 ± 0.01	0.16 ± 0.02	0.15 ± 0.01
2 Weeks post-MI	0.12 ± 0.01	0.13 ± 0.01	0.12 ± 0.02	0.11 ± 0.03	0.11 ± 0.02
*P** (Baseline vs. 2 weeks)	*< 0.01*	*< 0.01*	*< 0.01*	*< 0.0001*	*< 0.0001*
6 Weeks post-MI	0.11 ± 0.02	0.11 ± 0.01	0.13 ± 0.02	0.11 ± 0.03	0.12 ± 0.02
P† (Baseline vs. 6 weeks)	*< 0.001*	*< 0.0001*	*NS*	*< 0.0001*	*< 0.001*
P‡ (2 weeks vs. 6 weeks)	*NS*	*NS*	*NS*	*NS*	*NS*
IVSs (cm)					
Baseline	0.22 ± 0.03	0.20 ± 0.02	0.21 ± 0.02	0.22 ± 0.01	0.23 ± 0.01
2 Weeks post-MI	0.13 ± 0.02	0.13 ± 0.02	0.13 ± 0.02	0.12 ± 0.05	0.11 ± 0.04
*P** (Baseline vs. 2 weeks)	*< 0.0001*	*< 0.01*	*< 0.0001*	*< 0.0001*	*< 0.0001*
6 Weeks post-MI	0.10 ± 0.02	0.12 ± 0.02	0.18 ± 0.07$^{\#a,*b}$	0.11 ± 0.05	0.13 ± 0.04^{*a}
P† (Baseline vs. 6 weeks)	*< 0.0001*	*< 0.0001*	*NS*	*< 0.0001*	*< 0.0001*
P‡ (2 weeks vs. 6 weeks)	*NS*	*NS*	< 0.001	*NS*	*NS*
LVIDd (cm)					
Baseline	0.69 ± 0.06	0.70 ± 0.07	0.69 ± 0.06	0.71 ± 0.05	0.73 ± 0.04
2 Weeks post-MI	0.90 ± 0.09	0.84 ± 0.04	0.81 ± 0.09	0.84 ± 0.09	0.86 ± 0.06
P* (Baseline vs. 2 weeks)	*< 0.0001*	*< 0.0001*	*< 0.001*	*< 0.001*	*< 0.001*
6 Weeks post-MI	1.01 ± 0.07	0.92 ± 0.03	0.88 ± 0.08^{**a}	0.91 ± 0.07	0.90 ± 0.06^{*a}
P† (Baseline vs. 6 weeks)	*< 0.0001*	*< 0.0001*	*< 0.0001*	*< 0.0001*	*< 0.0001*
P‡ (2 weeks vs. 6 weeks)	*< 0.01*	*NS*	*NS*	*NS*	*NS*
LVIDs (cm)					
Baseline	0.44 ± 0.08	0.44 ± 0.07	0.43 ± 0.05	0.42 ± 0.04	0.44 ± 0.04
2 Weeks post-MI	0.75 ± 0.12	0.68 ± 0.07	0.65 ± 0.10	0.67 ± 0.13	0.74 ± 0.05
*P** (Baseline vs. 2 weeks)	*< 0.0001*	*< 0.0001*	*< 0.0001*	*< 0.0001*	*< 0.0001*
6 Weeks post-MI	0.85 ± 0.09	0.77 ± 0.05	0.67 ± 0.07$^{\#\#a,*b}$	0.75 ± 0.11	0.71 ± 0.03^{**a}
P† (Baseline vs. 6 weeks)	*< 0.0001*	*< 0.0001*	*< 0.0001*	*< 0.0001*	*< 0.0001*
P‡ (2 weeks vs. 6 weeks)	*< 0.05*	*< 0.05*	*NS*	*NS*	*NS*
FS (%)					
Baseline	37.0 ± 8.44	37.0 ± 5.12	38.2 ± 3.72	40.1 ± 2.72	41.3 ± 4.74
2 Weeks post-MI	17.7 ± 4.77	19.1 ± 6.96	20.0 ± 6.17	21.1 ± 8.25	18.5 ± 3.21
*P** (Baseline vs. 2 weeks)	*< 0.0001*	*< 0.0001*	*< 0.0001*	*< 0.0001*	*< 0.0001*
6 Weeks post-MI	15.6 ± 2.96	16.8 ± 4.84	24.5 ± 3.46^{**a,**b}	17.1 ± 5.49	23.2 ± 4.44^{**a,*c}
P† (Baseline vs. 6 weeks)	*< 0.0001*	*< 0.0001*	*< 0.0001*	*< 0.0001*	*< 0.0001*
P‡ (2 weeks vs. 6 weeks)	*NS*	*NS*	*NS*	*NS*	*NS*
EF (%)					
Baseline	77.1 ± 4.82	74.6 ± 6.25	76.2 ± 4.26	77.8 ± 3.32	78.7 ± 4.36
2 Weeks post-MI	43.8 ± 10.2	46.0 ± 13.0	48.0 ± 11.8	47.8 ± 12.1	43.3 ± 5.61
*P** (Baseline vs. 2 weeks)	*< 0.0001*	*< 0.001*	*< 0.0001*	*< 0.0001*	*< 0.0001*
6 Weeks post-MI	38.9 ± 6.85	41.1 ± 10.3	54.7 ± 9.6$^{\#a,*b}$	40.3 ± 11.7	46.0 ± 5.97^{*a}
P† (Baseline vs. 6 weeks)	*< 0.0001*	*< 0.0001*	*< 0.0001*	*< 0.0001*	*< 0.0001*
P‡ (2 weeks vs. 6 weeks)	*NS*	*NS*	*NS*	*NS*	*NS*
LVAd (cm^2)					
Baseline	0.45 ± 0.15	0.42 ± 0.11	0.39 ± 0.05	0.50 ± 0.05	0.50 ± 0.05
2 Weeks post-MI	0.69 ± 0.14	0.61 ± 0.08	0.62 ± 0.11	0.68 ± 0.13	0.68 ± 0.10
*P** (Baseline vs. 2 weeks)	*< 0.0001*	*< 0.001*	*< 0.001*	*< 0.01*	*< 0.001*
6 Weeks post-MI	0.81 ± 0.18	0.68 ± 0.07	0.65 ± 0.12	0.75 ± 0.14	0.69 ± 0.12
P† (Baseline vs. 6 weeks)	*< 0.0001*	*< 0.0001*	*< 0.0001*	*< 0.0001*	*< 0.001*
P‡ (2 weeks vs. 6 weeks)	*NS*	*NS*	*NS*	*< 0.01*	*NS*
LVAs (cm^2)					
Baseline	0.16 ± 0.07	0.19 ± 0.06	0.16 ± 0.04	0.21 ± 0.03	0.19 ± 0.05
2 Weeks post-MI	0.41 ± 0.13	0.38 ± 0.04	0.39 ± 0.09	0.44 ± 0.11	0.45 ± 0.09
*P** (Baseline vs. 2 weeks)	*< 0.0001*	*< 0.001*	*< 0.0001*	*< 0.01*	*< 0.001*
6 Weeks post-MI	0.54 ± 0.18	0.45 ± 0.07	0.39 ± 0.09^{*a}	0.49 ± 0.12	0.46 ± 0.08
P† (Baseline vs. 6 weeks)	*< 0.0001*	*< 0.0001*	*< 0.0001*	*< 0.0001*	*< 0.001*
P‡ (2 weeks vs. 6 weeks)	*< 0.01*	*NS*	*NS*	*NS*	*NS*

(*continued*)

Supplementary Table S1. (Continued)

	MI (n = *8*)	*FG* (n = *8*)	*SASG* (n = *8*)	*FG-VATS* (n = *7*)	*SASG-VATS* (n = *8*)
FAC (%)					
Baseline	59.0 ± 5.13	58.6 ± 4.84	59.7 ± 5.96	57.2 ± 4.75	61.0 ± 9.35
2 Weeks post-MI	33.1 ± 3.84	36.5 ± 4.72	37.1 ± 3.28	35.7 ± 5.38	33.6 ± 4.34
P^* (Baseline vs. 2 weeks)	*< 0.0001*	*< 0.0001*	*< 0.0001*	*< 0.0001*	*< 0.0001*
6 Weeks post-MI	28.9 ± 5.79	31.1 ± 7.14	41.6 ± 4.74$^{\#a,*b}$	34.5 ± 5.49	35.8 ± 2.22
$P^\dagger$ (Baseline vs. 6 weeks)	*< 0.0001*	*< 0.0001*	*< 0.0001*	*< 0.0001*	*< 0.0001*
$P^\ddagger$ (2 weeks vs. 6 weeks)	*NS*	*NS*	*NS*	*NS*	*NS*

Values are presented as mean ± SD.

P^*, *P*-values derived from paired comparisons between baseline and 2 weeks after MI measurements.

$P^\dagger$, *P*-values derived from paired comparisons between baseline and 6 week after MI (4 weeks after treatment) measurements.

$P^\ddagger$, *P*-values derived from paired comparisons between 2 weeks (pre-treatment) and 6 weeks after MI (4 weeks post-treatment) measurements.

Group-time interaction:

$^{*a}P < 0.05$ versus MI.

$^{**a}P < 0.01$ versus MI.

$^{\#a}P < 0.001$ versus MI.

$^{\#\#a}P < 0.0001$ versus MI.

$^{*b}P < 0.05$ versus FG.

$^{**b}P < 0.005$ versus FG.

$^{*c}P < 0.05$ versus FG-VATS.

VATS, video-assisted thoracoscopic surgery; LV, left ventricular; MI; myocardial infarction; IVSd, LV wall thickness/interventricular septum dimensions in diastole; IVSs, LV wall thickness/interventricular septum dimensions in systole; LVIDd, LV end internal dimension in diastole; LVIDs, LV end internal dimension in systole; FS, LV fractional shortening; EF, LV ejection fraction; LVAd, LV area in diastole; LVAs, LV area in systole, FAC, LV fractional area change; FG, fibrin graft; SASG, subamnion-cord-lining mesenchymal stem cells angiogenic spheroids-enriched graft; FG-VATS, FG generated in situ via VATS; SASG-VATS, SASG generated in situ via VATS.

were acquired at 0.5 μm intervals using a Nikon A1R confocal microscope, and subsequently processed using NIS-Elements software (v 3.1, Nikon).

LV blood vessel density was also quantified in all animals using Masson's trichrome-stained sections. The number of total blood vessels and arterioles (i.e., 5–50 μm diameter blood vessels displaying a smooth muscle media layer) [10,11] was determined in the border zone and infarcted myocardium. Myocardium extending 0.5–1.0 mm from the infarcted tissue or infarct scar was considered to represent the border zone myocardium[12]. Micrographs from 10 random high-power fields per zone (400×) were taken. All quantifications were done using Image J software.

References

1. Cheong HH, J Masilamani, TT Phan and SY Chan. (2010). Cord lining progenitor cells: potential in vitro adipogenesis model. Int J Obes 34:1625–1633.
2. Kofidis T, JL de Bruin, G Hoyt, DR Lebl, M Tanaka, T Yamane, CP Chang and RC Robbins. (2004). Injectable bioartificial myocardial tissue for large-scale intramural cell transfer and functional recovery of injured heart muscle. J Thorac Cardiovasc Surg 128:571–578.
3. Deuse T, M Stubbendorff, K Tang-Quan, N Phillips, MA Kay, T Eiermann, TT Phan, HD Volk, H Reichenspurner, RC Robbins and S Schrepfer. (2011). Immunogenicity and immunomodulatory properties of umbilical cord lining mesenchymal stem cells. Cell Transplant 20:655–667.
4. Martinez EC, J Wang, SU Gan, R Singh, CN Lee and T Kofidis. (2010). Ascorbic acid improves embryonic cardiomyoblast cell survival and promotes vascularization in potential myocardial grafts in vivo. Tissue Eng Part A 16:1349–1361.
5. Martinez EC, J Wang, S Lilyanna, LH Ling, SU Gan, R Singh, CN Lee and T Kofidis. (2013). Post-ischaemic angiogenic therapy using in vivo prevascularized ascorbic acid-enriched myocardial artificial grafts improves heart function in a rat model. J Tissue Eng Regen Med 7:203–212.
6. Weytjens C, B Cosyns, J D'Hooge, C Gallez, S Droogmans, T Lahoute, P Franken and G Van Camp. (2006). Doppler myocardial imaging in adult male rats: reference values and reproducibility of velocity and deformation parameters. Eur J Echocardiogr 7:411–417.
7. Takagawa J, Y Zhang, ML Wong, RE Sievers, NK Kapasi, Y Wang, Y Yeghiazarians, RJ Lee, W Grossman and ML Springer. (2007). Myocardial infarct size measurement in the mouse chronic infarction model: comparison of area- and length-based approaches. J Appl Physiol 102: 2104–2111.
8. Nascimento DS, M Valente, T Esteves, F de Pina Mde, JG Guedes, A Freire, P Quelhas and OP Pinto-do. (2011). MI-Quant—semi-automation of infarct size assessment in models of cardiac ischemic injury. PLoS One 6:e25045.
9. Li Y, Y Song, L Zhao, G Gaidosh, AM Laties and R Wen. (2008). Direct labeling and visualization of blood vessels with lipophilic carbocyanine dye DiI. Nat Protoc 3:1703–1708.
10. Al-Khaldi A, N Eliopoulos, D Martineau, L Lejeune, K Lachapelle and J Galipeau. (2003). Postnatal bone marrow stromal cells elicit a potent VEGF-dependent neoangiogenic response in vivo. Gene Ther 10:621–629.
11. Crottogini A, PC Meckert, G Vera Janavel, E Lascano, J Negroni, H Del Valle, E Dulbecco, P Werba, L Cuniberti, et al. (2003). Arteriogenesis induced by intramyocardial vascular endothelial growth factor 165 gene transfer in chronically ischemic pigs. Hum Gene Ther 14:1307–1318.
12. Jin P, E Wang, YH Wang, W Huang, W Kuang, C Sun, S Hu and H Zhang. (2012). Central zone of myocardial infarction: a neglected target area for heart cell therapy. J Cell Mol Med 16:637–648.
13. Kelm JM, C Diaz Sanchez-Bustamante, E Ehler, SP Hoerstrup, V Djonov, L Ittner and M Fussenegger. (2005). VEGF profiling and angiogenesis in human microtissues. J Biotechnol 118:213–229.